Journal of Catalysis **211,** 407–421 (2002)
doi:10.1006/jcat.2002.3719

Reduction and Oxygen Storage Behavior of Noble Metals Supported on Silica-Doped Ceria

Eliana Rocchini,* Michela Vicario,* Jordi Llorca,† Carla de Leitenburg,* Giuliano Dolcetti,* and Alessandro Trovarelli*,[1]

*Dipartimento di Scienze e Tecnologie Chimiche, Università di Udine, Via del Cotonificio 108, 33100 Udine, Italy; and †Departament de Química Inorgànica, Universitat de Barcelona, Diagonal 647, 08028 Barcelona, Spain

Received March 18, 2002; revised May 30, 2002; accepted May 30, 2002

The redox features of Rh and other noble metals (Pt, Pd) supported on silica-doped ceria catalysts are investigated by temperature-programmed reduction (TPR) and temperature-programmed oxidation (TPO). Noble metal oxides are reduced to the corresponding metals at temperatures below 600 K, whereas at higher temperatures the reduction of the support takes place with formation of reduced ceria and a cerium silicate phase. After redox aging, reduction of the support in the bulk occurs at lower temperatures; this effect depends on the amount of silicon present. A more detailed reduction profile is obtained by monitoring water evolution during TPR in both ceria and ceria-silica-based catalysts. Differences are observed in H_2 consumption and water formation which are not always simultaneous: their positions depend on redox treatments, precursor salt used for preparation, and type of support. Oxidation of CO under oscillating feedstream conditions is used as an estimate of dynamic oxygen storage capacity. Redox treatment promotes oxygen storage on both the support and noble-metals-supported samples. This is related to the formation during reduction of a silicate phase, as evidenced by X-ray diffraction and HRTEM analysis, which on reoxidation gives small particles of nanocrystalline ceria.

Key Words: **rhodium; platinum; palladium; Rh/CeO_2; CeO_2-SiO_2; ceria; TWC; TPR; oxygen storage capacity; three-way catalysts; ceria–zirconia.**

1. INTRODUCTION

The redox chemistry of ceria is a critical parameter in the efficiency of multifunctional components of three-way automotive catalysts. The main function of ceria is to provide an oxygen buffering capacity during excursion of the air/fuel ratio into a rich or lean regime. This derives from the ability of CeO_2 to be easily reduced giving an extended range of possible stoichiometries CeO_{2-x} with $0 < x < 0.5$. Although only a small fraction of this range is effectively used during operation of three-way catalysts ($0 < x < 0.02$), the study of reduction of ceria and its interaction with hydrogen under more or less severe conditions has represented a major effort in the last decade (1). These studies are critically reviewed in a number of recent surveys (2, 3). In short, the main findings can be summarized as follows: (i) ceria is reduced by hydrogen at temperatures higher than 600 K and reduction is strongly affected by textural (4–7); (ii) irreversible and reversible reduction (i.e., reduction with and without water/vacancy formation) have been observed to occur depending on several variables like pretreatments, precursor salts, presence of noble metals, etc. (2, 8); (iii) the presence of noble metals dramatically changes the redox behavior due to hydrogen activation by the metal at lower temperature and consequent migration to the support (spillover) favoring reduction of the surface (9–11); (iv) incorporation of transition-metal elements into CeO_2 lattice (particularly Zr) can deeply influence reduction under hydrogen by promoting reduction of the bulk at lower temperature (3); (v) incorporation of hydrogen by ceria during reduction has been reported to occur although this phenomenon has given rise to discussion and controversy in the literature (4, 12–16); and (vi) the effect of pretreatments and metal precursors (nitrates, chlorides, etc.) can strongly modify the redox behavior (17–19).

Current investigations focus on improving the low-temperature redox efficiency and the thermal stability of materials containing ceria. Several studies reported the use of iso- and aliovalent cations such as Zr^{4+}, Si^{4+}, La^{3+}, Tb^{3+}, and Pr^{3+} as dopant agents for ceria providing enhanced thermal stabilization and/or improved oxygen storage capacities (OSCs) (20–28). We recently found that, under specific conditions, silica positively affects the redox behavior of ceria (29), resulting in an enhancement of its reduction properties even after a strong redox treatment, a condition that heavily inhibits reduction in pure ceria (30). This occurs in a fashion similar to that observed earlier by doping ceria with zirconia (24), although the origin of this behavior is completely different. Several hypotheses have been put forward to explain the higher reducibility of ceria–zirconia compared to ceria (3). In summary, it seems that the promotion of the reduction behavior in ceria–zirconia

[1] To whom correspondence should be addressed. Fax: +39-0432-558803. E-mail: trovarelli@dstc.uniud.it.

0021-9517/02 $35.00

depends on structural perturbation in the lattice of ceria induced by the dopant. In the case of ceria–silica, the origin of this promotion depends on the formation of a new phase/compound whose rearrangement induces stabilization of small ceria crystallites. Evidence for formation of $Ce_{9.33}(SiO_4)_6O_2$ under reducing conditions was obtained by electron microscopy and X-ray diffraction (29). The formation of this phase enables the limitations imposed by thermodynamics in the reduction of ceria to be overcome and almost 80% of cerium formally shifts to the 3+ oxidation state in the form of cerium silicate. On reoxidation, this phase decomposes giving amorphous silica and small ceria crystallites, which are much more reactive toward reduction and oxidation. In addition, it is known that SiO_2 is also an effective surface-area-stabilizing agent for ceria, as previously reported by Rhône-Poulenc researchers (31, 32).

The current investigation concentrates on the effect of silicon on the redox properties of ceria in the presence of Rh and other noble metals (NM), like Pt and Pd. In particular, we describe here the redox behavior of NM/CeO_2–SiO_2 and its dependence on composition, pretreatment, and the structural modifications that occur on the support. The dynamics of CeO_2–SiO_2 and NM/CeO_2–SiO_2 transformations were studied by means of temperature-programmed reduction/oxidation (TPR/TPO), X-ray powder diffraction studies, and BET and high-resolution transmission electron microscopy (HRTEM) analysis. We also investigated the oxygen storage/release properties of these materials in comparison with undoped ceria by carrying out CO oxidation under oscillating feedstream conditions.

2. EXPERIMENTAL

2.1. Materials

The synthesis and structural characterization of the supports were previously reported (29). Briefly, the supports containing various amounts of silica were obtained by coprecipitation after hydrothermal synthesis in a Nalgene autoclave. A solution of sodium silicate was added to an aqueous solution of $CeCl_3 \cdot 7H_2O$ and precipitation was obtained by addition of an aqueous solution of NH_3. Table 1 details the characteristics of the supports used in this study.

After calcination of the supports at 923 K for 2 h, NM loading (1 wt%) was obtained by incipient wetness using aqueous solutions of $Pd(NO_3)_2$, H_2PtCl_6 (Johnson Matthey), $RhCl_3 \cdot 3H_2O$, and $Rh(NO_3)_3$ (Aldrich). After impregnation, the catalysts were dried at 393 K overnight and calcined at 923 K for 2 h in a tubular oven (⊘ 50-mm length, 900-mm) under an air flow of 0.2 L/min (STP).

The specific surface areas of oxide powders were measured by the BET method using N_2 adsorption/desorption at 77 K with a Sorptomatic 1990 instrument (Carlo Erba).

TABLE 1

Characteristics of Ceria–Silica Samples

Sample	Composition (wt%) CeO_2	Composition (wt%) SiO_2	Si (wt%) nominal (found)	Si/Ce molar ratio	Surface area (m^2/g)
CS0	100	0	0 (0.02)	0	77
CS02	99.6	0.4	0.2 (0.33)	0.01	117
CS1	97.9	2.1	1 (1.18)	0.06	131
CS3	93.6	6.4	3 (3.17)	0.19	155
CS6	87.2	12.8	6 (5.49)	0.42	168

2.2. Reduction and Oxidation Studies

TPR was carried out in a flow system by placing the catalyst (50 mg) in a U-shaped quartz reactor heated by a furnace from 298 K (243 K for low-temperature TPR) to 1400 K at 10 K/min and using a gas mixture (5% H_2 in argon) flowing at 35 ml/min. Before measurements, the samples were first oxidized in air by heating at 10 K/min from room temperature to 923 K and then were maintained at this temperature for 1 h. TPO was carried out in a flow system in which the gas mixture (1% O_2 in He) was passed at 35 ml/min over 150-mg samples using a tubular quartz reactor. The reactors were placed in a furnace, which was programmed to heat at a rate of 10 K/min from 298 to 1400 K. Gas analysis was performed using a thermal conductivity detector for TPR (TPR/TC) or a quadrupole mass spectrometer (Balzers) for TPO (TPO/MS). Hydrogen consumption in TPR was standardized by the reduction of CuO to metallic copper.

Redox behavior was checked by running two consecutive TPRs, separated by an oxidation treatment of 1 h under air at 773 K. The second TPR was chosen as an indicator of the response of the catalyst to severe reduction/oxidation treatments (redox cycle).

Technical limitations of conventional TPR technique have already been pointed out and concern mainly the modification of H_2-consumption profiles due to desorption and reaction of surface impurities (33); additional limiting factors arise from the lack of quantitative data regarding water production during reduction. This does not allow one to distinguish if H_2 consumption originates from reduction and/or adsorption/incorporation processes. The use of a mass spectrometer detector partly overcomes these limitations and semiquantitative data can be obtained (34). However, the lower sensitivity and some dilution and mass selection effects can often be observed during capillary sampling, which does not allow precise quantitative analysis of peak shape and position. To allow a more precise quantitative monitoring of effluents and lack of mass-selection effect during sampling, a series of TPRs were carried out by a modification of the standard TPR apparatus with the introduction of a micro-GC detector which allows complete

analysis of effluents (including CO and CO_2 originating from carbonate impurities) in less than 80 s (TPR/μGC experiments). Thus a complete TPR profile can be collected in the range 298–1273 K with an accuracy of approximately 10 K in the determination of peak position. A comparison between the quantity and position of H_2 consumption and H_2O evolution peaks enables one to distinguish between the extent of reduction and of any H_2 incorporation phenomena.

2.3. Oxygen Storage Measurements

OSC under dynamic conditions was measured by a reactor working in cycling mode, following a method already reported by Boaro *et al.* (27). Samples were placed in a quartz microreactor (9-mm o.d. by 6-mm i.d. by 440-mm length) vertically located at the center of a furnace, and the catalyst temperature was maintained between 298 and 1273 K. A chromel–alumel thermocouple inside the reactor was used to measure the catalyst inlet temperature (i.e., reaction temperature). The powdered catalyst was loaded together with quartz beads ($300 < ? < 630$ μm) sustained in the reactor by a quartz-wool bed. During reaction, the samples were exposed to alternating 2% O_2 and 4% CO in He pulses of 1-s duration, each separated by a 1-s pulse of helium to ensure complete flushing of gas-phase species between pulses (total flow 120 ml/min). The same experiments were repeated, changing the pulse frequency from 1 to 0.2 Hz, to study the subsurface oxygen mobility of the catalysts. Average concentration of the outlet mixture was simultaneously analyzed by a flame ionization detector equipped with a methanation reactor and a thermal conductivity detector of an HP 5890 gas chromatograph. Instantaneous composition was followed by a fast inlet quadrupole mass spectrometer (Hiden Analytical HPR20) located just following the reactor.

2.4. Characterization of Materials

X-ray powder diffraction profiles were collected with a Siemens 700 instrument, using a Ni-filtered Cu target. For *in situ* oxidation studies a Paar HTK 10AP high-temperature chamber was used. Conventional transmission electron microscopy combined with energy-dispersive X-ray microanalysis was performed using a Hitachi MT-800 electron microscope working at 200 kV and equipped with a Kevex analytical system and a built-in CCD camera. Microstructural characterization by HRTEM was carried out with a Philips CM-30 instrument operating at 300 kV with 0.20-nm point-to-point resolution. Samples were placed on copper grids with a holey carbon film by depositing a drop of the specimen suspended in methanol. The experimental image was digitalized on a high-resolution scanner, and digital processing was performed with a local software package.

3. RESULTS

3.1. Temperature-Programmed Reduction and Oxidation Studies

3.1.1. Temperature-programmed reduction studies (TPR/TC) with Rh-containing samples. Figure 1 shows the reduction profiles of Rh (1 wt%) deposited on CeO_2 and CeO_2–SiO_2. The profile relative to Rh/CeO_2 (Fig. 1, curve e_1) is characterized by two peaks (1), one low-temperature peak due to reduction of Rh_2O_3 to Rh and one high-temperature peak due to support reduction. Calculation of H_2 uptake from the first peak (see Table 2) indicates a consumption of 335 μmol H_2/g_{CeO_2}, which is higher than the 146 μmol H_2/g_{CeO_2} expected for the reduction of all the rhodium oxide to the metal state. The difference can be accounted for by the hydrogen adsorption that occurs on both the metal and the support. It is very well known that Rh/CeO_2 reduced at moderate temperature shows the occurrence of strong spillover phenomena (10, 35) even at room or near room temperature. We also observed a strong decrease in H_2 adsorption at low temperature if the Rh/CeO_2 catalyst was subjected to a redox cycle, i.e., an initial TPR followed by reoxidation at 773 K (Fig. 1, curve

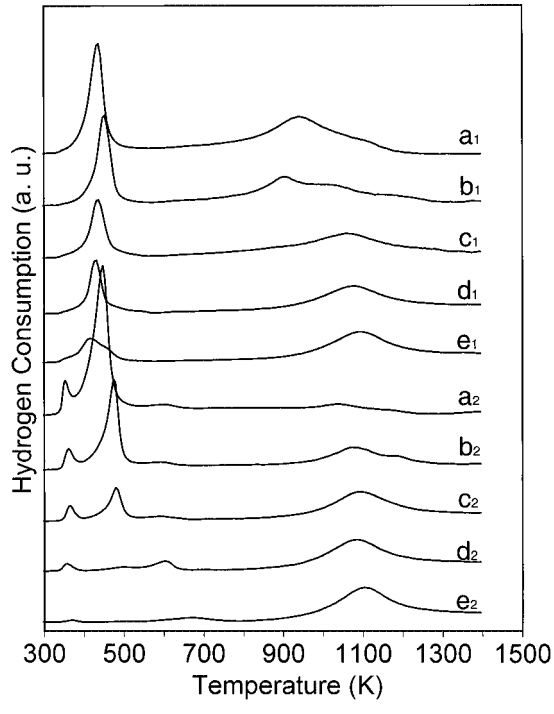

FIG. 1. TPR profiles of Rh-supported on CeO_2–SiO_2: (a_1) fresh Rh/CS6, (a_2) sample resulting from experiment a_1 further reoxidized at 773 K, (b_1) fresh Rh/CS3, (b_2) sample resulting from experiment b_1 further reoxidized at 773 K, (c_1) fresh Rh/CS1, (c_2) sample resulting from experiment c_1 further reoxidized at 773 K, (d_1) fresh Rh/CS02, (d_2) sample resulting from experiment d_1 further reoxidized at 773 K, (e_1) fresh Rh/CS0, (e_2) sample resulting from experiment e_1 further reoxidized at 773 K.

TABLE 2

Hydrogen Consumption of Rh/CS Samples under TPR Conditions

		First TPR[a]			Second TPR		
Sample	Rh[b]	LTP	Total	x	LTP	Total	x
Rh/CS6	167	1037	2703	1.52	1815	2269	1.60
Rh/CS3	156	774	2264	1.60	981	1994	1.65
Rh/CS1	149	549	1885	1.67	430	1668	1.71
Rh/CS02	146	426	1705	1.70	106	1522	1.73
Rh/CS0	146	335	1658	1.71	21	1412	1.75

[a] Consumption of H_2 (μmol/$g_{cat.}$) measured during the first TPR: total consumption calculated at 1400 K (Total), consumption under low-temperature peak (LTP), value of x in CeO_x calculated after first TPR.

[b] Calculated hydrogen consumption due to Rh present on the support according to the following reaction: $Rh_2O_3 + 3H_2 = 2Rh + 3H_2O$.

e_2). In this case, a value of 21 μmol H_2/g_{CeO_2} was measured, which was lower than the 146 expected for reduction. The difference may be attributed to one or more of the following reasons: (i) the presence of well-dispersed Rh_2O_3 that can be reduced at subambient temperature and escapes TPR detection (36), (ii) the suppression of H_2 spillover from the metal to the support (10), (iii) the encapsulation of metal particles following the high-temperature aging treatment (37), and (iv) the occurence of decoration phenomena of SMSI-like origin (38). Reduction at subambient temperature of well-dispersed Rh_2O_3 is unlikely because of the severe aging treatment (first TPR up to 1400 K and reoxidation at 773 K), which causes sintering of metal particles; it was excluded by starting the second TPR from 243 K instead of 298 K. This did not evidence any further consumption of H_2 at low temperature. Decoration phenomena are produced by reduced support particles which migrate on the top of metal particles during reduction (1, 2, 38). This phenomenon is observed in pure ceria after reduction at high temperatures and is normally reversed under oxidizing atmospheres. In our case, the persistence of decoration after a redox cycle cannot be excluded if the intermediate reoxidation is carried out at 773 K. It is reported that only reoxidation at higher temperatures should cause a complete reversal of any metal decoration phenomena induced by reduced moieties coming from the support (38). It is therefore likely that the decrease in hydrogen consumption in the second TPR originates from a cooperative effect deriving from blockage of the spillover phenomenon and residual decoration of the metal which persists after mild reoxidation. Reduction treatment during the first TPR induces a notable decrease in the catalyst surface area to values lower than 5–10 m^2/g. Consequent to this support sintering, there would be some metal loss via an encapsulation process. This additional effect could contribute to reducing H_2 adsorption by decreasing the available metal surface area and by blocking the spillover phenomenon. In addition, the spillover rate is influenced by the degree of hydroxilation of the support (10), which, in the case of a redox-aged catalyst, is certainly low. In our opinion, this additional effect also reinforces our previous suggestion.

The incorporation of silica into the support leads to several modifications in the reduction behavior of both ceria and rhodium (Fig. 1 curves a_1–d_1). Consumption of H_2 for Rh_2O_3 reduction during the first TPR increases with the presence of SiO_2 up to a value of 1037 μmol H_2/g_{CeO_2} observed for Rh/CS6; this value is further incremented after high-temperature redox aging, especially for Rh/CS6, in contrast with the value observed on Rh/CSX with $X < 3$. In addition, consumption of H_2 for high-temperature reduction in this sample is strongly reduced. While the behavior during the first TPR can be easily explained by an increase in spillover phenomena due to the high surface area of silica-containing samples and by the high degree of hydroxilation of these samples, the situation following the redox cycle deserves further comments. The very low surface area of the samples after the redox cycle (surface area is lower than 5–10 m^2/g in all samples investigated) means that a rough estimation of H_2 necessary for reduction of ceria surface will be ca. 8 μmol of H_2 per square meter of available CeO_2 surface. This can be calculated by the application of a linear relationship between surface area and H_2 consumption (15). This is, of course, an upper limit since it does not take into account that some ceria is covered by metal and/or by silica, and is therefore not accessible by the gas phase. Consequently, the low-temperature peak for a silicon content higher than 0.2 wt% includes a contribution of H_2 consumption/adsorption for reduction in the bulk of the material. This contribution rises as the amount of silica increases. The phenomenon can also be inferred from the lack of substantial H_2 consumption at high temperature, where the bulk ceria support is normally reduced. A contribution to H_2 consumption at low temperature might also occur because of H_2 dissolution into the lattice of CeO_2 without reduction, as reported previously by Fierro *et al.* (16). The presence of silica thus promotes interaction of H_2 with ceria in the bulk at much lower temperatures after a high-temperature redox-aging procedure, and the best behavior is observed with CS6. This was therefore the support we selected as a reference for a more detailed reduction study.

3.1.2. Temperature programmed reduction studies (TPR/μGC) with Rh-containing samples. To better clarify the nature of H_2–CeO_2 interaction in the Rh/CS6 system we carried out a series of TPRs using a micro-GC as a detector to allow for monitoring and quantification of evolved water. Figure 2 shows H_2 consumption and H_2O evolution profiles in the TPR of fresh and redox-aged ceria and ceria–silica. In all cases evolution of water occurs "in phase" with H_2 consumption indicating that H_2 is consumed for

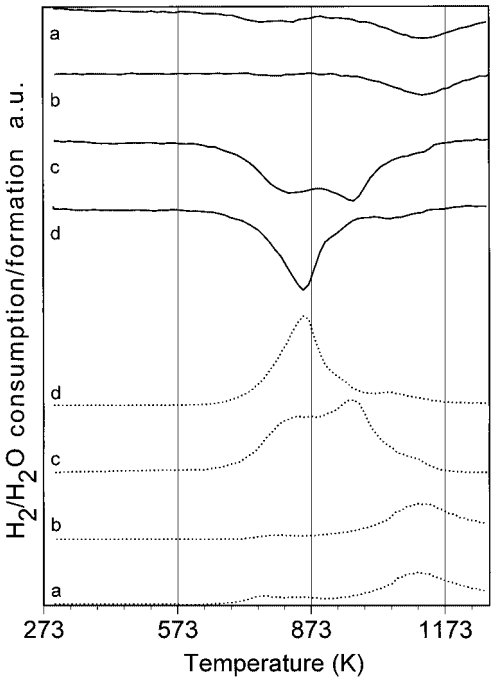

FIG. 2. Profiles of H_2 uptake (solid line) and H_2O evolution (dotted line) obtained in TPR-μGC of (a) fresh CS0, (b) CS0 after a redox cycle, (c) fresh CS6, and (d) CS6 after a redox cycle.

irreversible reduction of the support with vacancy formation. Quantitative data are reported in Table 3. The degree of irreversible reduction obtained with pure ceria at 1273 K is close to that observed at these temperatures in the literature (7, 11) and corresponds to formation of CeO_x with $x = 1.82$ and 1.85 respectively for fresh and redox-aged material. Reduction calculated from water evolution does not modify this figure, thus excluding any major H_2 inclusion or incorporation phenomena under these conditions. This is also in agreement with the results obtained by Kondarides and Verykios who found no H_2 desorption from ceria in H_2-TPD (18). A higher reduction degree of ceria is reached in CS6, as already observed (25). Also in this case, quantitative analysis does confirm that H_2 is not adsorbed or stored in the support under TPR conditions.

TPR with monitoring of evolved water was also carried out on fresh and redox-cycled Rh/CS0 and Rh/CS6 samples. In this case we used both chloride (Cl) and nitrate (N) Rh precursors since it was reported that this could affect reduction performances (8, 34). The main features confirm results obtained with conventional TPR analysis (Fig. 3). In Rh/CS6 prepared either from chlorides or nitrates, reduction of cerium is promoted compared to Rh/CS0 in redox-cycled samples, as confirmed by the absence of the high-temperature peak due to reduction of bulk cerium atoms (compare profiles e and f). The behavior of fresh and redox-cycled Rh/CS0 is reported in profiles c, d, g, and h. Reduction shows similar profiles for the two treatments. Consumption of H_2 and water formation occurs

TABLE 3

Quantitative Data Regarding H_2 Consumption and Water Evolution after TPR/μGC Studies

Sample	x in CeO_x[a]	
	H_2	H_2O
Fresh CS0	1.82	1.83
Redox-cycled CS0	1.85	1.85
Fresh CS6	1.62	1.63
Redox-cycled CS6	1.70	1.72
Fresh Rh(Cl)/CS0	1.72	1.69
Redox-cycled Rh(Cl)/CS0	1.78	1.76
Fresh Rh(N)/CS0	1.82	1.83
Redox-cycled Rh(N)/CS0	1.88	1.85
Fresh Rh(Cl)/CS6	1.56	1.52
Redox-cycled Rh(Cl)/CS6	1.53	1.50
Fresh Rh(N)/CS6	1.56	1.57
Redox-cycled Rh(N)/CS6	1.54	1.56

[a] Values of x in CeO_x calculated at the end of TPR/μGC (1273 K) from H_2 evolution and H_2O formation.

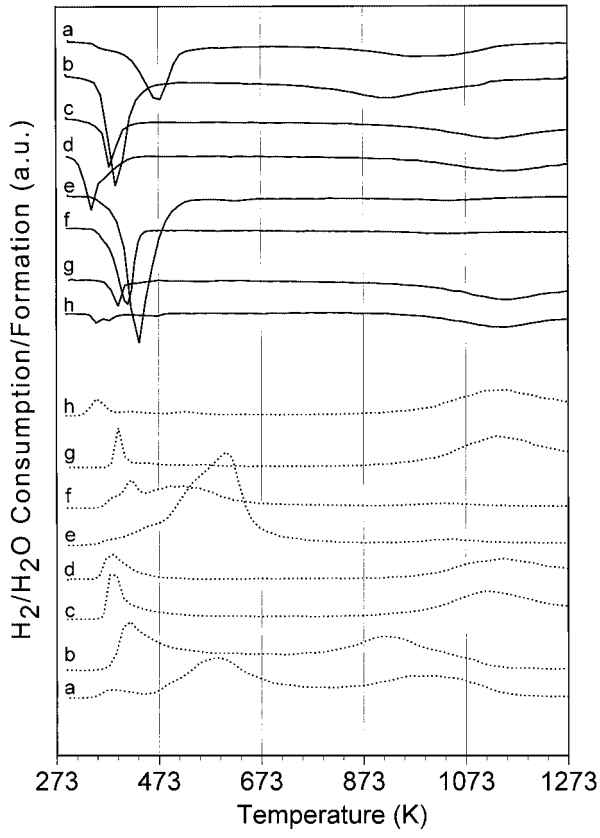

FIG. 3. Profiles of H_2 uptake (solid line) and H_2O evolution (dotted line) obtained in TPR/μGC of (a) fresh Rh(Cl)/CS6, (b) fresh Rh(N)/CS6, (c) fresh Rh(Cl)/CS0, (d) fresh Rh(N)/CS0, (e) Rh(Cl)CS6 after a redox cycle, (f) Rh(N)/CS6 after a redox cycle, (g) Rh(Cl)/CS0 after a redox cycle, and (h) Rh(N)/CS0 after a redox cycle.

simultaneously with fresh Rh(Cl)/CS0 (profiles c), while a small anticipation of H_2 consumption is observed in fresh Rh(N)/CS0 (profiles d). For recycled samples this anticipation is lost in agreement with results of Fornasiero *et al.* (34) who found inhibition of H_2 adsorption at low temperature in Rh(N)/CeO_2–ZrO_2 after redox aging. The introduction of SiO_2 modifies profiles of H_2 adsorption in agreement with TPR/TC measurements. In addition, in the presence of chlorides the main low-temperature reduction peak is shifted to higher temperatures and is not in phase with H_2O evolution; that is, H_2 consumption occurs before H_2O evolution (compare profiles a and e). This behavior is particularly evident after a redox cycle. In this case H_2 is activated for Rh_2O_3 reduction (the water formation peak for Rh_2O_3 reduction is observed as a small shoulder at lower temperature) and then it is stored in some form up to where irreversible reduction of ceria occurs at temperatures between 550 and 600 K. A similar shift to higher temperature is observed in the reduction of bulk Ce(IV) for fresh Rh(Cl)/CS6 compared to samples prepared from nitrates. Quantitative data reported in Table 3 indicate that the final reduction degree strongly depends on sample, pretreatment, and precursor used for metal deposition. The overall reduction degree calculated from H_2 consumption and H_2O evolution is in good agreement, indicating that the estimate of final reduction degree from H_2 consumption is reasonable if done on the entire TPR profile. (The situation is different if intermediate reduction degrees are evaluated on the basis of H_2 consumption only, due to H_2 adsorption phenomena and to reversible and irreversible reduction which can take place also simultaneously.) As a general trend with Cl-containing samples, a much deeper reduction degree is obtained with Rh/CS0, in agreement with previous studies (8), while with silica-containing samples this difference is less important.

3.1.3. TPR studies with NM-containing samples. Figure 4 compares the reduction features of Rh, Pt, and Pd supported on CS6. The first profiles (a_1–d_1) relate to fresh samples while profiles a_2–d_2 refer to catalysts subjected to a redox-aging cycle. For comparison, traces belonging to CS6 before (a_1) and after redox cycle (a_2) are also reported. As already shown, profile b_1 has two peaks. One, located at 430 K, belongs to the reduction of the rhodium oxide to rhodium metal and to the surface reduction of the support at lower temperatures via a spillover effect, whereas the other peak is due to support reduction. The other metals show similar characteristics: H_2 uptake for platinum reduction, trace c_1, occurs at 560 K while palladium, trace d_1, has a reduction peak centered at ca. 390 K. The difference in the position of the peaks can be related to precursors utilized for metal deposition and to the characteristics of noble metals. The higher reduction temperature of platinum oxide in Pt/CS6 is probably due to the presence of platinum oxychloride [$Pt^{IV}O_xCl_y$] formed by interaction of Pt with residual chloride, which cannot be totally eliminated by the relatively mild pretreatment conditions employed in this study. Reduction of the oxychloride is reported to occur at ca. 200 K higher than that of α-[PtO_2] surface species, which reduces at about 400 K (39). Hydrogen consumption for reduction of Pt and Pd oxides is reported in Table 4. Hydrogen consumption at low temperature is higher than the amount required for metal reduction only, indicating

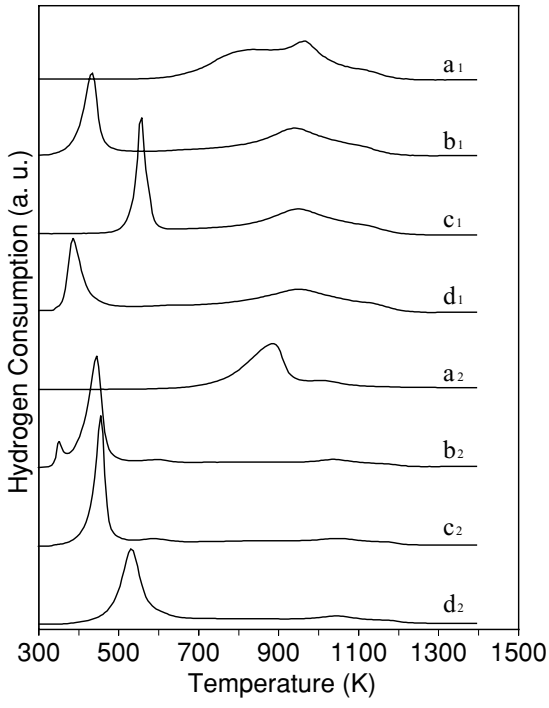

FIG. 4. TPR profiles of bare and supported CS6: (a_1) fresh CS6, (a_2) sample resulting from experiment a_1 further reoxidized at 773 K, (b_1) fresh Rh/CS6, (b_2) sample resulting from experiment b_1 further reoxidized at 773 K, (c_1) fresh Pt/CS6, (c_2) sample resulting from experiment c_1 further reoxidized at 773 K, (d_1) fresh Pd/CS6, (d_2) sample resulting from experiment d_1 further reoxidized at 773 K.

TABLE 4

Hydrogen Consumption of Pt- and Pd-Supported Samples under TPR Conditions

		First TPR[a]			Second TPR		
Sample	NM[b]	LTP	Total	x[c]	LTP	Total	x
Pt/CS6	118	1027	2513	1.56	1495	2191	1.62
Pt/CS0	103	205	1495	1.74	60	1440	1.75
Pd/CS6	108	933	2494	1.57	1683	2171	1.62
Pd/CS0	94	144	1497	1.74	60	1469	1.74

[a] Consumption of H_2 (μmol/$g_{cat.}$) measured during the first TPR: total consumption calculated at 1400 K (Total), consumption under low-temperature peak (LTP), value of x in CeO_x calculated after first TPR.

[b] Calculated hydrogen consumption due to noble metal present on the support according to the presence of Rh_2O_3, PtO_2, and PdO.

[c] x in CeO_x calculated at the end of TPR/TC.

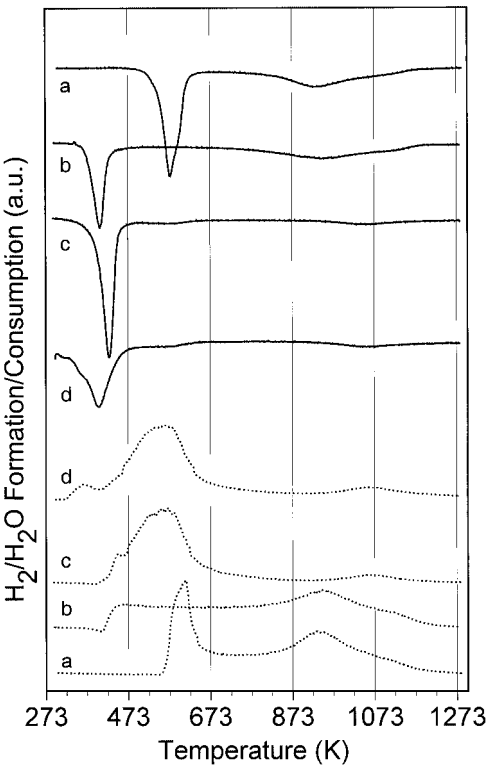

FIG. 5. Profiles of H_2 uptake (solid line) and H_2O evolution (dotted line) obtained in TPR/μGC of (a) fresh Pt/CS6, (b) fresh Pd/CS6, (c) redox-aged Pt/CS6, and (d) redox-aged Pd/CS6.

the occurrence of spillover. The second peak at ca. 950 K is due to the bulk reduction of the support and is observable in traces a_1–d_1. After redox cycle, the TPR of the unsupported oxide shows a profile with one major peak centered at ca. 880 K. There is residual H_2 consumption at higher temperatures. As observed with Rh, H_2 consumption for metal-supported samples at low temperature increases and a decrease in the intensities of the high-temperature peak to very low values is also observed. Reduction profiles with water analysis does confirm the main reduction findings (Fig. 5). Hydrogen consumption and water formation are in phase with fresh Pt/CS6 and Pd/CS6 catalyst while during the second TPR there is a high temperature shift in water evolution at low temperature indicating that reversible and irreversible reduction occur in two distinct intervals.

For comparison, the same experiments were carried out on Rh, Pt, and Pd supported on pure CeO_2 prepared using the same experimental procedure but without silicon (Fig. 6). Traces a_1–d_1 show the TPR experiments carried out on the fresh samples including the support. The H_2 consumption splits into two peaks, a low-temperature peak due to metal reduction and a peak at ca. 1100 K due to reduction of bulk CeO_2 to CeO_{2-x}. Qualitatively, the profiles resemble those in Fig. 4 but with a decrease in intensity of H_2 consumption associated with metal reduction peaks and an increase in those associated with support reduction. This is due to the lower surface area of CS0 compared to the silica-doped counterpart, which decreases the amount of hydrogen activated by the metal and is used for support reduction at low temperature. The second TPR following reoxidation of sample at 773 K shows striking differences. The low-temperature peak due to H_2 consumption for noble-metal reduction is no longer visible. Treatment under H_2 at high temperature causes a drop in ceria surface area down to a few square meters per gram (29). It is likely that the loss in surface area at the end of the first TPR promotes an almost total encapsulation of the metal within the sintered support, as already reported (24). As a result, metal particles are not exposed to the reducing atmosphere during the oxidation and second TPR. Reduction does not, therefore, proceed. The possibility of subambient reduction of the metal was ruled out by running TPR starting from 243 K. To study how the reoxidation temperature affects the redox behavior, a series of TPRs were carried out on the reference Rh/CS6 sample by changing the intermediate reoxidation temperature (Figs. 7A and 7B). The following treatments were performed sequentially: TPR of the fresh Rh/CS6 sample (Fig. 7A, profile a), TPR of sample a after reoxidation at 1073 K for 1 h under air (profile b), TPR of sample b after reoxidation at 773 K for 1 h under air

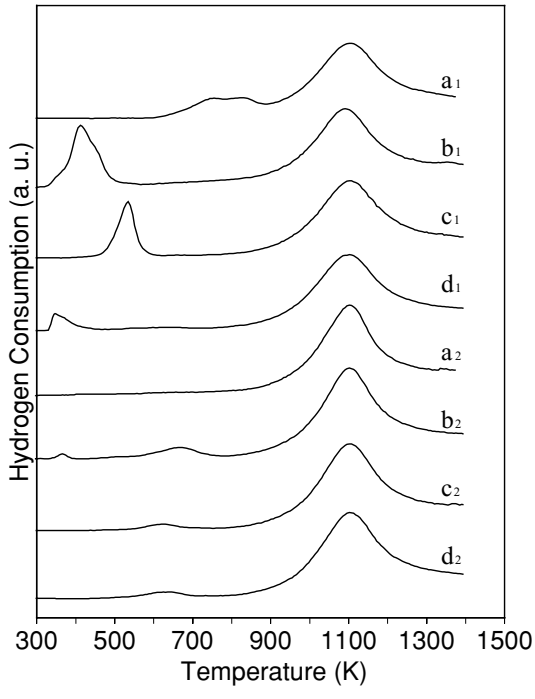

FIG. 6. TPR profiles of bare and supported CS0: (a_1) fresh CS0, (a_2) sample resulting from experiment a_1 reoxidized at 773 K, (b_1) fresh Rh/CS0, (b_2) sample resulting from experiment b_1 reoxidized at 773 K, (c_1) fresh Pt/CS0, (c_2) sample resulting from experiment c_1 reoxidized at 773 K, (d_1) fresh Pd/CS0, (d_2) sample resulting from experiment d_1 reoxidized at 773 K.

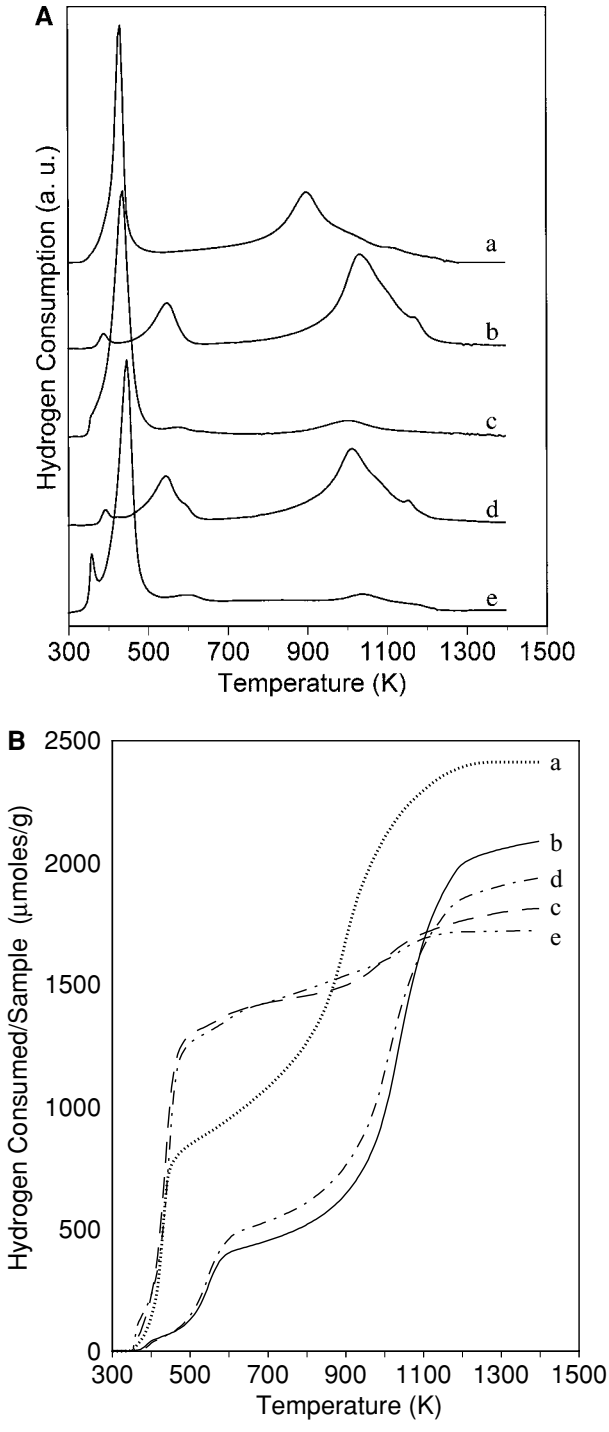

FIG. 7. (A) TPR profiles of (a) fresh Rh/CS6 calcined at 923 K, (b) sample resulting from (a) reoxidized at 1073 K, (c) sample resulting from (b) reoxidized at 773 K, (d) sample resulting from (c) reoxidized at 1073 K, and (e) sample resulting from (d) reoxidized at 773 K. (B) Hydrogen consumption calculated for profiles reported in (A).

(profile c), TPR of sample c after reoxidation at 1073 K for 1 h under air (profile d), TPR of sample d after reoxidation at 773 K for 1 h under air (profile e). It should be observed that after reoxidation at 1073 K, the TPR traces are very different from those obtained after reoxidation at 773 K. The peak due to metal reduction shifts to higher temperature and its intensity strongly decreases, whereas the intensity of the high-temperature peak increases. This behavior is totally reversible by repeating TPR profiles and varying the intermediate oxidation temperature (see profiles b–e). Quantitative details of this behavior are reported in Fig. 7B, where hydrogen consumption is calculated from reduction of Rh/CS6 subjected to different reoxidation temperatures. A comparison of traces c and e with traces b and d indicates that intermediate oxidation at 773 K strongly promotes low-temperature reduction (ca. 1300 μmol $H_2/g_{cat.}$ were consumed at a temperature of 500 K) while oxidation at 1073 K causes a remarkable drop of hydrogen consumption at these temperatures (at 500 K, less than 200 μmol $H_2/g_{cat.}$). In contrast, the total degree of reduction is only slightly modified by varying reoxidation temperature.

3.1.4. Temperature-programmed oxidation (TPO/MS) studies. To better understand how the reoxidation phenomenon affects subsequent reduction, a series of TPOs were carried out on bare and Rh-supported samples of CS0–CS6 following pre-reduction by TPR (Figs. 8A and 8B). Whereas with pure ceria, or ceria doped with small amounts of SiO_2, reoxidation takes place at low temperature ($T < 400$–450 K), in the presence of larger amounts of SiO_2 reoxidation progressively shifts to higher temperatures with broad peaks located in the ranges 300–500 K and 1000–1100 K (samples d and e in Fig. 8A). Figure 8B presents the oxidation profiles of rhodium supported on samples previously reduced by TPR. A series of peaks are observable. The peak at 350 K is easily attributed to the reoxidation of the CeO_{2-x} phase (17). The small peak at 723 K belongs to the reoxidation of the metallic rhodium (40) and the decomposition of Rh_2O_3 is shown at about 1300 K. The remaining peaks in the range 300–600 K, 1020 K (in trace d), and 1100 K (in trace e) are due to the reoxidation phenomena involving the cerium silicate phase, which forms under reductive conditions (29). It is important to emphasize that while the reduction process of ceria with rhodium takes place at lower temperatures, there is no such enhancement in the case of oxidation.

3.2. Oxygen Storage Measurements

While TPR studies are generally a good estimate of total oxygen storage capacity, their effectiveness in predicting or extrapolating the behavior of materials under dynamic conditions is rather limited (41). In addition, OSC results are influenced by the type of reductant used, and the oxygen available for redox cycling can be quite different if measured using H_2 or CO. To support TPR data for dynamic applications, we therefore carried out oxygen storage measurements under oscillating conditions by feeding CO and O_2 alternately to the reactor, separated by pulses of He, as described in the experimental section. Data were analyzed

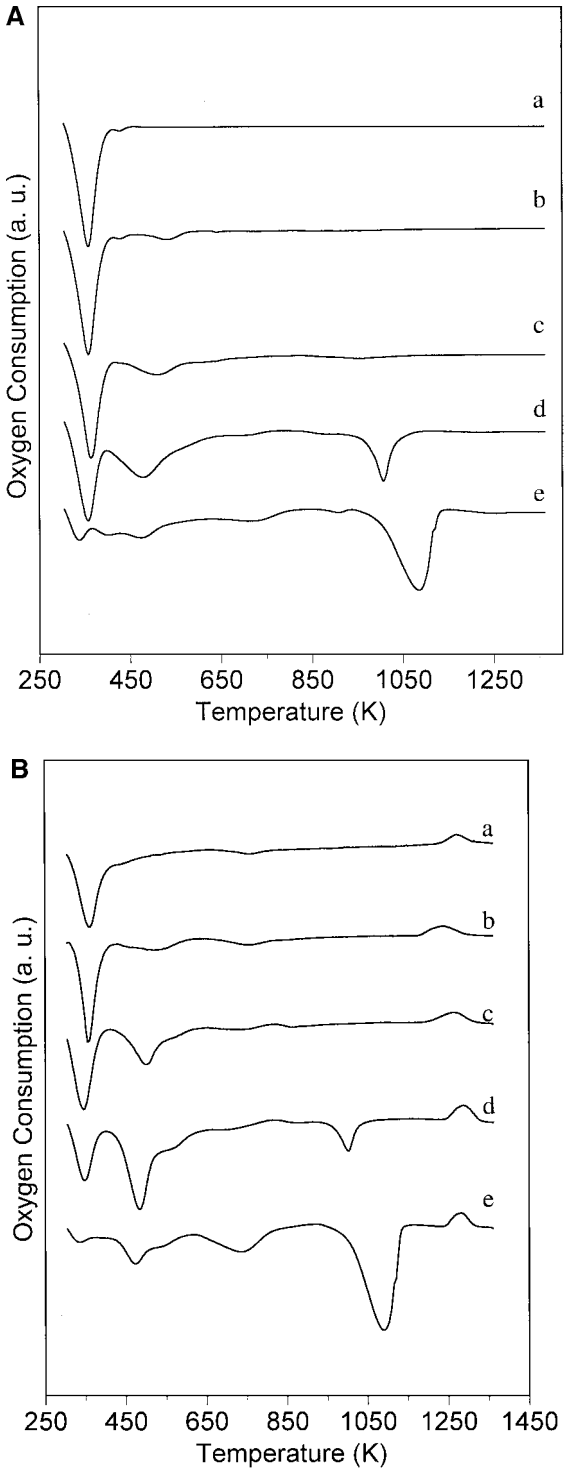

FIG. 8. (A) TPO profiles of samples after TPR: (a) CS0, (b) CS02, (c) CS1, (d) CS3, and (e) CS6. (B) TPO profiles of (a) Rh/CS0, (b) Rh/CS02, (c) Rh/CS1, (d) Rh/CS3, and (e) Rh/CS6.

in terms of light-off curves showing the average CO conversion vs. temperature for Rh-free and metal-supported samples at different oscillation frequencies. Figure 9 shows the results for the supports at a feeding frequency of 1 and 0.2 Hz. As a general trend, there is a loss of overall activity as measured by the light-off temperature (i.e., temperature at 50% CO conversion; see Table 5) on increasing the excursion time to rich/lean composition from 1 to 5 s. Similar behavior is observed on redox-aged samples, where an increase between 100 and 200 K in the light-off temperature is shown compared to fresh samples. For fresh samples feeding at 1 Hz, the order of activity is CS0 > CS3 > CS6. This is maintained even at 0.2 Hz, although the difference between CS0 and CS6 is much narrower and activity is almost identical. After redox aging, an inversion is observed and the CS6 sample is more active than CS0, especially at 0.2 Hz, where a difference of more than 100 K is observed in the light-off temperature. This picture is consistent with TPR results that indicate a promotion of reduction behavior in CS6 compared to CS0 after redox aging even under dynamic conditions. It is likely to originate from the participation of oxygen subsurface layers in CO oxidation. After aging, the surface of the catalyst drops to less than 5 m^2/g, making the contribution of oxygen from the lattice much more significant.

The introduction of Rh lowers the light-off temperature of fresh catalysts and promotes CO oxidation over CS6 compared to CS0 (Fig. 10). The activity is higher at 0.2 Hz, which can be explained by the participation of Rh in the oxygen transfer from the lattice to the gas phase under reducing conditions, as first described by Bunluesin *et al.* (42). The phenomenon is more pronounced after redox aging, where the activity of Rh/CS6 is even higher than that of fresh Rh/CS0 at high temperature. The very low activity of Rh/CS0 after redox aging can be explained by a greater encapsulation of Rh into the support following high-temperature treatment, which is also supported by TPR analysis.

3.3. Structural Characterization

To obtain more information about the structural modifications that occur on NM supported on silica-doped samples during reduction and reoxidation treatments, we investigated the sample Rh/CS6, chosen as representative, by using X-ray powder diffraction and combined HRTEM and energy dispersive X-ray analysis (EDX). In Fig. 11, the X-ray diffraction profile recorded at 298 K for

TABLE 5

Light-off Temperatures

	T (50%), 1 Hz			*T* (50%), 0.2 Hz		
Sample	Fresh	Aged	ΔT	Fresh	Aged	ΔT
CS0	690	910	220	760	970	210
CS6	780	902	122	800	850	50
Rh/CS0	648	865	217	510	740	230
Rh/CS6	610	710	100	470	550	80

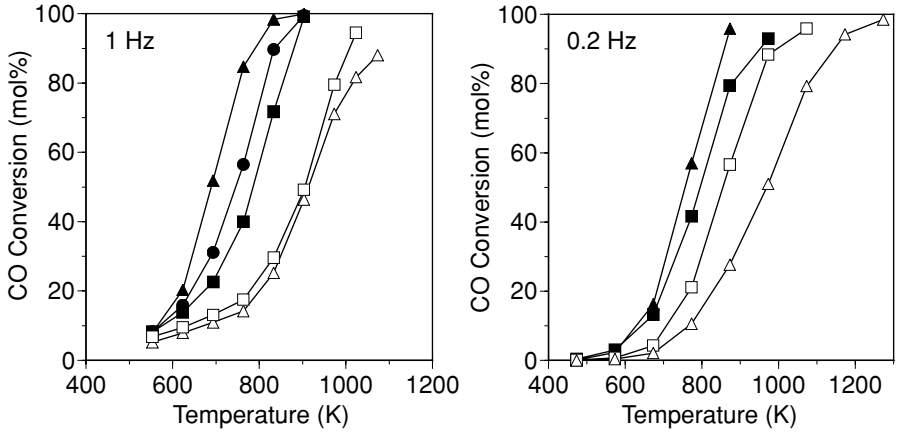

FIG. 9. Left: CO conversion vs. temperature for CeO_2–SiO_2. Catalyst wt. 60 mg, cycling frequency 1 Hz; fresh samples (▲) CS0, (●) CS3, (■) CS6 and samples after redox aging, (□) CS6, (△) CS0. Right: CO conversion vs. temperature for CeO_2–SiO_2. Catalyst wt. 150 mg, cycling frequency 0.2 Hz. Fresh samples (▲) CS0, (■) CS6 and samples after redox aging (□) CS6, (△) CS0.

the Rh/CS6 sample obtained after hydrogen treatment at 1373 K shows the presence of a hexagonal phase belonging to $Ce_{9.33}(SiO_4)_6O_2$, the same one recorded with Rh-free CS6 sample (29). Upon calcination *in situ*, the hexagonal phase fully transforms to cubic ceria. Between 298 and 873 K, the hexagonal phase progressively vanishes, giving rise to an amorphous structure that is particularly visible at 873 K. Between 873 and 1073 K, this amorphous phase converts to pure ceria with a much smaller crystallite size in comparison with that of bulk ceria not involved in transformation with silica. With CS6, the stoichiometry of CeO_2 reaction with SiO_2 involves the reaction of ca. 65 wt% of ceria with all silica present according to the formal reaction:

$$9.33CeO_2 + 6SiO_2 + 4.66H_2 = Ce_{9.33}(SiO_4)_6O_2 + 4.66\,H_2O$$

All these observations are similar to those already obtained for CS6, so the presence of rhodium does not appear to affect these phase transformations under the conditions used in this work. No Rh-based phases are detected by XRD due to low metal loading (1 wt%).

Structural changes were also investigated by electron microscopy. Fig. 12 illustrates an HRTEM image corresponding to the CS6-supported rhodium catalyst reduced at 1373 K under TPR conditions. A rhodium crystallite with a particle size of about 4.5 nm is clearly visible. The inset in this image shows the electron diffraction pattern recorded for the support alone, which is oriented along the [1 1 $\bar{2}$ 1] crystallographic direction. The cell parameters obtained from different electron diffraction patterns for the hexagonal $Ce_{9.33}(SiO_4)_6O_2$ support phase are $a = b = 9.61$ Å, $c = 7.13$ Å. The occurrence of an epitaxial relationship consisting of the parallel growth of planes of metallic rhodium and the support is suggested from this and other HRTEM

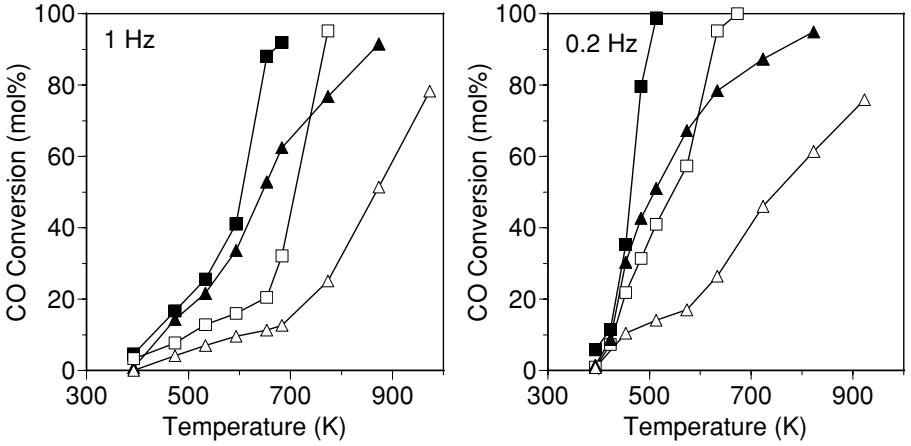

FIG. 10. Left: CO conversion vs. temperature for Rh/CeO_2–SiO_2. Catalyst wt. 10 mg, cycling frequency 1 Hz; fresh samples (■) CS6, (▲) CS0 and samples after redox-aging cycle (□) CS6, (△) CS0. Right: CO conversion vs. temperature for Rh/CeO_2–SiO_2. Catalyst wt. 130 mg, cycling frequency 0.2 Hz; fresh samples (■) CS6, (▲) CS0 and samples after redox aging (□) CS6, (△) CS0.

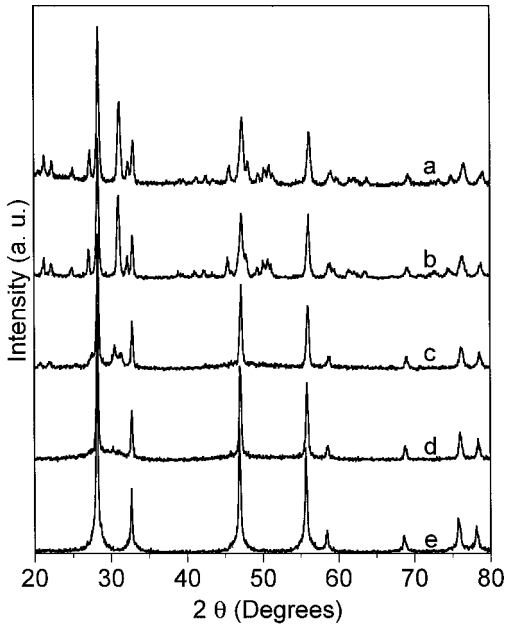

FIG. 11. X-ray powder diffraction patterns of (a) Rh/CS6 reduced at 1373 K, (b) Rh/CS6 reoxidized at 473 K, (c) Rh/CS6 reoxidized at 673 K, (d) Rh/CS6 reoxidized at 873 K, and (e) Rh/CS6 reoxidized at 1073 K.

images. Furthermore, a metal decoration phenomenon is observed to occur on all the CS6-supported rhodium crystallites of the sample obtained after reduction at 1373 K (see also Fig. 13). Clean and well-faceted rhodium crystallites are totally absent. A detailed analysis of the decoring phase carried out in reciprocal space shows that it consists of pure CeO_2 and not $Ce_{9.33}(SiO_4)_6O_2$. This is nicely represented in Figs. 12 and 13, where lattice fringes at 3.12–3.13 Å on the top of the rhodium crystallites are indicative of CeO_2 (111) planes. From these high-resolution images, it is proposed that metal decoration by the support takes place by virtue of a process consisting of CeO_2 segregation and migration on top of rhodium crystallites, rather than by the penetration of the metal particles into the support. Covering of rhodium particles by CeO_2 has been observed to occur in a similar way in ceria-supported Rh catalysts at reduction temperatures higher than 973 K, and much more heavily on samples reduced at 1173 K (35).

After reoxidation at 773 K, sample Rh/CS6 contains a mixture of CeO_2, cerium silicate phase, SiO_2, and particles containing rhodium. Figure 14 shows all these components in a low-magnification HRTEM image. The occurrence of pure CeO_2 is clear from Fig. 14 (parts A and B) where a spacing corresponding to CeO_2 (200) planes at 2.7 Å are present. In addition, the occurrence of the $Ce_{9.33}(SiO_4)_6O_2$ phase is clearly visible in Fig. 14, part C, where a crystal of $Ce_{9.33}(SiO_4)_6O_2$ is present along the crystallographic direction [1 1 $\bar{2}$ 0]. On top of both CeO_2 and $Ce_{9.33}(SiO_4)_6O_2$, there are Rh-containing particles, as determined by EDX. The exact nature of these particles (Rh or Rh oxides) is impossible to ascertain because of the presence of a layer of amorphous silica that hinders lattice fringe images. It appears that the Rh particles have, in fact, suffered from the redox treatments and have broken apart.

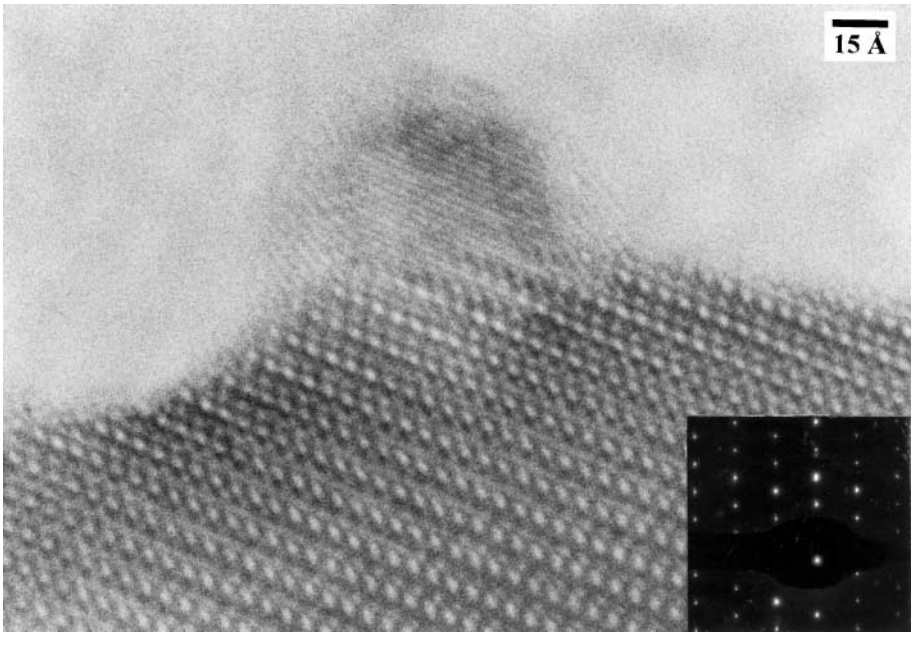

FIG. 12. HRTEM image in profile view of the Rh/CS6 catalyst reduced at 1373 K. Inset: selected area electron diffraction (SAED) pattern of the support. Rhodium (111) planes at 2.2 Å grow parallel to (100) planes of $Ce_{9.33}(SiO_4)_6O_2$ at 8.4 Å CeO_2 planes at 3.13 Åare visible on the top left of the rhodium crystallite.

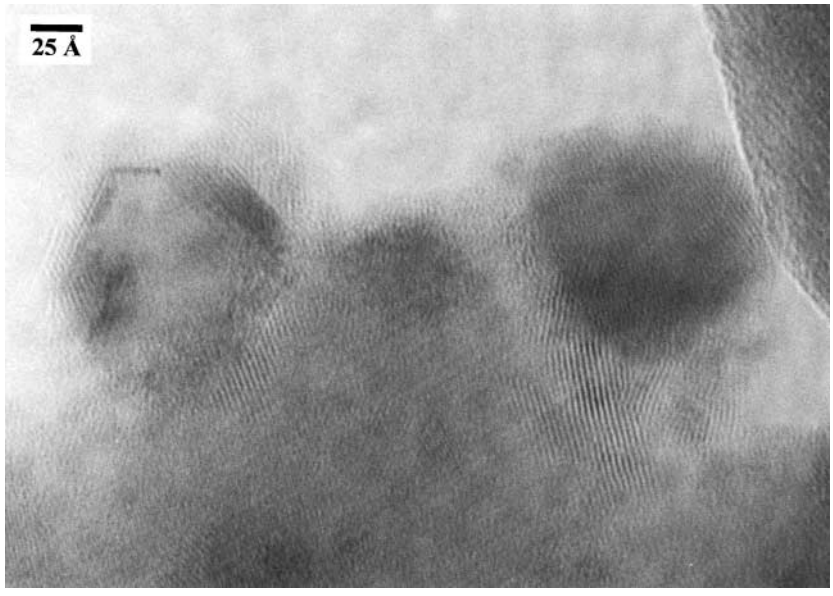

FIG. 13. HRTEM image of the Rh/CS6 catalyst reduced at 1373 K. Metal particles appear to be covered by CeO_2.

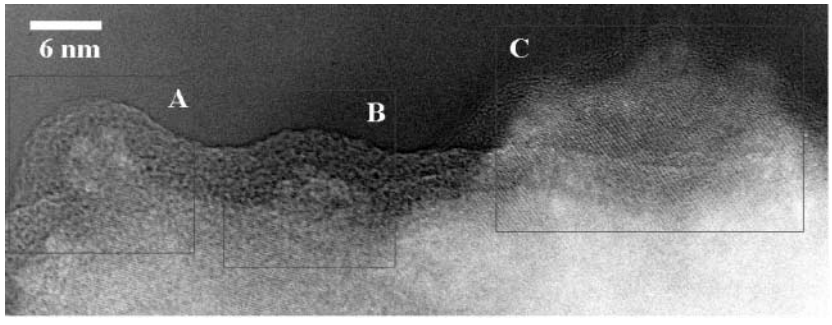

FIG. 14. HRTEM image of the Rh/CS6 catalyst reduced at 1373 K and reoxidized at 773 K. Areas A and B show rhodium particles supported on ceria and covered by a layer of amorphous silica. Inset C shows rhodium particles supported on $Ce_{9.33}(SiO_4)_6O_2$ and covered by a layer of amorphous silica.

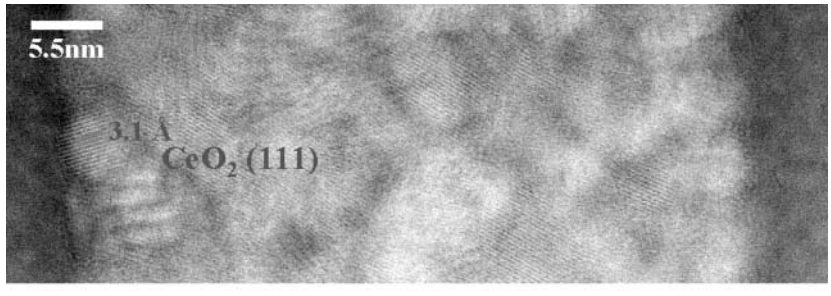

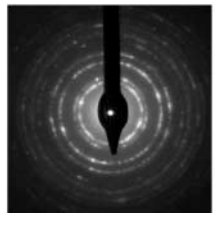

FIG. 15. HRTEM image of the Rh/CS6 catalyst reduced at 1373 K and reoxidized at 1073 K. Ceria particles are embebbed in amorphous silica. SAED pattern exhibits rings corresponding to pure CeO_2.

When the reoxidation treatment is carried out at 1073 K, there is a complete transformation of the $Ce_{9.33}(SiO_4)_6O_2$ phase into CeO_2 microcrystallites, as occurs in the absence of Rh (compare also TPR analysis). Figure 15 shows a selected-area electron diffraction (SAED) pattern along a general high-resolution view of a representative part of the sample. The rings correspond to pure fcc CeO_2 and there are no diffraction rings corresponding to $Ce_{9.33}(SiO_4)_6O_2$. One crystal of CeO_2 is marked in Fig. 15, showing CeO_2 planes at 3.2 Å. The exact location of Rh was not determined due to the presence of amorphous silica.

4. DISCUSSION

The results presented in this paper show that under certain conditions, the reduction behavior and oxygen storage properties of Rh/CeO_2–SiO_2 improve after redox treatment at high temperature. It is generally recognized that treatment at high temperature under H_2 strongly affects the reduction properties of NM/CeO_2 catalysts, which is indicated by the loss of low-temperature reduction features of ceria. This is a consequence of the blocking of the spillover phenomena and of partial encapsulation of the metal in the sintered support (1–3).

We have recently shown that the doping of CeO_2 with low amounts of silica strongly modifies redox behavior, leading to an enhancement of bulk ceria reduction at low temperature (29). This occurs in a fashion similar to that observed by doping with ZrO_2. However, the origin of this promotion does not depend on structural perturbation in the ceria lattice induced by the dopant but on the formation of a new phase/compound which then rearranges, stabilizing small ceria crystallites. Evidence for the formation of $Ce_{9.33}(SiO_4)_6O_2$ under reducing conditions was obtained by HRTEM and XRD. The formation of this phase means that the limitations in ceria reduction imposed by thermodynamics can be overcome and almost 80% of cerium formally shifts to the 3+ oxidation state in the form of cerium silicate. On reoxidation, this phase decomposes to give amorphous silica and small ceria crystallites, which are much more reactive to reduction and oxidation. This implies that the thermodynamics of the reduction process is more favorable on small ceria crystallites because of lower reduction enthalpy (43). The presence of noble metals induces several modifications to the reduction profiles of the support (i) by increasing SiO_2 content, an increase in H_2 consumption at low temperature is observed; (ii) for some compositions, a change in the reduction features is associated with redox treatments (the second TPR shows an enhancement of both irreversible and reversible reduction in the low-temperature range); and (iii) the behavior of the second TPR is strongly affected by intermediate reduction. Let us analyze in more detail the likely origin of these features. It is well known that spillover phenomena affect the low-temperature reduction profile of a Rh/CeO_2 catalyst, or more generally of NM/CeO_2 (1, 2). This occurs because H_2 is activated by the metal site and is then spilled over the surface of the support, where reversible/irreversible reduction of the more reducible surface sites occurs at much lower temperature. This explains why in all samples investigated (Rh/CS0–Rh/CS6), consumed hydrogen calculated under the first low-temperature peak is higher than the theoretical amount calculated on the basis of Rh oxide reduction. The question whether this H_2 consumption is correlated with irreversible reduction (i.e., formation of oxygen vacancies) can be addressed by looking at the position of water evolution peaks, which in the case of Rh/CeO_2, are quite coincident with peaks of H_2 consumption (compare H_2/H_2O profiles c, d, g, and h in Fig. 3). Samples prepared by nitrates show a little shift of water evolution peak at higher temperature compared to hydrogen adsorption. This can be explained by a higher tendency of these samples to be reversibly reduced first (compared to Cl-containing samples) and only in a successive step they are reduced with formation of vacancies (8).

With samples containing silica, hydrogen consumption rises and can be associated with an increase in available surface Ce sites as a consequence of the larger surface area available in the presence of silica (see Table 1). This increases the amount of H_2 reversibly adsorbed on the surface because the difference in the position of H_2 consumption and H_2O formation in the TPR is more relevant. This can be correlated to the presence of small ceria particles more prone to reduction. Total reduction is also affected by Si; with the Rh/CS6 sample, almost all the Ce^{4+} present is reduced to Ce^{3+} at the end of the first TPR. It is suggested that this second step is a result of the reduction of bulk Ce^{4+} to Ce^{3+} driven by the formation of the $Ce_{9.33}(SiO_4)_6O_2$ phase. The peculiar behavior shown during the second TPR can be explained by keeping in mind the structural and morphological modifications of the support that occur during the redox treatment. After the first TPR, treatment at high temperature under H_2 causes a drop in surface area of all the catalysts investigated. This should cause an almost parallel decrease in H_2 adsorption/spillover, as observed on Rh/CS0 and Rh/CS02. For all the other samples, the amount of H_2 consumed is higher than the theoretical amount and for samples Rh/CS3 and Rh/CS6, is even higher than that observed after the first TPR. As evidenced by previous analysis of supports (29) and by present HRTEM and XRD data on Rh-containing samples, reduction leads to the formation of the $Ce_{9.33}(SiO_4)_6O_2$ phase which, upon reoxidation at 773 K, originates small CeO_2 crystallites and amorphous silica. The small ceria crystallites are easily reduced, even in the bulk, during the second TPR by spillover H_2 at low temperature. Bulk reduction of ceria is in fact greatly facilitated by the smaller dimensions of the crystallites. By lowering Si content, as in the presence of pure ceria, no such

small crystallites are present and reduction is strongly retarded. Moreover, the structural rearrangement observed upon reoxidation of Rh/CS6, which assists in the formation of CeO_2 and SiO_2 from the cerium silicate, helps in avoiding encapsulation of the metal. The presence of silica also favors the reversal of SMSI-like decoration phenomena already after reoxidation at 773 K, where Rh is free from particles of reduced support, in contrast to what observed in Rh/CeO_2 where decoration persists even after oxidation at higher temperatures (38, 44). Therefore the formation of cerium silicate during the reduction step allows the development upon reoxidation of small ceria particles that in the presence of Rh are reduced at low temperature (almost 60% of CeO_2 is reduced at a temperature lower than approx. 600 K). If reoxidation at intermediate temperatures is carried out at 1073 K, this promotion is lost (see Fig. 7B) because of sintering of these small ceria crystallites. In addition to these rearrangements it is also likely that silica migration to the surface might well affect changes in reducibility of different samples and/or samples exposed to different reoxidation environments. As observed in HRTEM section a surface layer of amorphous silica is present at the top of Rh and ceria crystallites as a result of structural rearrangement following redox treatment. This would cause a decrease of available surface Ce sites, depending on the amount of silica and on the extent of surface migration, thus changing the extent of Ce reduction as a function of reoxidation temperature. As suggested by a referee, the migration of silica to the surface would also affect spillover rate with a subsequent modification of overall H_2 consumption during low-temperature reduction.

Promotion of reduction at low temperature does not necessarily mean that oxygen storage behavior follows the same trend. Recently, limitations of TPR measurements in the estimate of oxygen storage has been demonstrated by Hickey *et al.* (41). In this study it was shown that despite the favorable reduction behavior observed in TPR of ceria–zirconia samples, oxygen storage measured under dynamic conditions revealed a strong deactivation. In the current study we have compared the reduction behavior of ceria-containing samples with CO oxidation. It is observed that high-temperature redox aging always causes a deactivation of CO oxidation measured under dynamic conditions, regardless of the samples investigated, in contrast to what happens by looking at the effect of redox aging on the reduction behavior only. However, it is observed that the presence of silica has a positive influence after redox aging compared to ceria-only catalysts. Thus, while for fresh catalysts CS0 performs better than CS6, for aged catalysts the situation is reversed and light-off temperatures for silica-doped samples are lower than those observed on undoped ceria. The higher CO oxidation activity of fresh CS0 compared to fresh CS6 can be explained by a higher concentration of redox-active Ce^{4+}/Ce^{3+} sites on the surface in the absence of silica. After redox treatment the situation is reversed and the stabilization of small crystallites in silica-containing samples helps CO oxidation. This is better evidenced by gas mixtures oscillating at lower frequency (i.e., 0.2 Hz rather than 1 Hz) and it indicates the importance of the balance between kinetic and thermodynamic factors in the overall behavior of TPR and OSC (7).

The presence of the metal does not greatly affect this picture; Rh catalysts deposited on silica-containing supports are less affected by redox-aging procedure. We have interpreted the difference in OSC activity of redox-aged samples as the result of several factors: (i) a different degree of surface area loss after reduction with different degrees of Rh encapsulation; (ii) the persistence of decoration phenomena established during reduction and not completely reversed after mild reoxidation in the absence of silica (as previously pointed out encapsulation/decoration phenomena after reoxidation are certainly less important in Rh/CS6 sample); and (iii) the stabilization of small ceria crystallites under mild reoxidation conditions.

In summary, we have found that oxygen exchange (either during reduction with hydrogen or during CO oxidation) is promoted if ceria is modified by the presence of silica. This promotion is much more evident after redox aging due to the formation of small ceria crystallites. It is difficult to discuss how and to what extent these features will help OSC for a real system. However, OSC under real-environment conditions will certainly benefit from the following characteristics of a ceria–silica system: (i) H_2/H_2O adsorption features at low temperature: CeO_2 is an active catalyst for the water gas shift reaction (1) and a better OSC is expected at low temperature by forming hydrogen from CO when water is present; (ii) easy recovery from encapsulation/decoration phenomena during reaction; and (iii) activity is less affected by aging and therefore greater durability is expected in a redox environment. An important limitation currently is the reoxidation temperature which cause growth of ceria crystallites already at 1073 K with a resulting drop of oxygen storage activity.

ACKNOWLEDGMENTS

The authors thank CNR, MURST, and Regione Friuli Venezia Giulia for financial support. J. Llorca is grateful to MCYT for a Ramón y Cajal research program. We also thank Johnson Matthey for a gentle loan of Pd.

REFERENCES

1. Trovarelli, A., *Catal. Rev.—Sci. Eng.* **38**(4), 439 (1996).
2. Bernal, S., Calvino, J. J., Gatica, J. M., López Cartes, C., and Pintado, J. M., *in* "Catalysis by Ceria and Related Materials" (A. Trovarelli, Ed.), Catalytic Science Series—Vol. 2, Chap. 4, pp. 85–168. Imperial College Press, London, 2002.
3. Kaspar, J., Fornasiero, P., and Graziani, M., *Catal. Today* **50**, 285 (1999).
4. Bernal, S., Calvino, J. J., Cifredo, G. A., Gatica, J. M., Pérez Omil, J. A., and Pintado, J. M., *J. Chem. Soc., Faraday Trans.* **89**, 3499 (1993).

5. Perrichon, V., Laachir, A., Abouarnadasse, S., Touret, O., and Blanchard, G., *Appl. Catal., A: General* **129**, 69 (1995).
6. Bruce, L. A., Hoang, M., Hughes, A. E., and Turney, T. W., *Appl. Catal., A: General* **134**, 351 (1996).
7. Giordano, F., Trovarelli, A., de Leitenburg, C., and Giona, M., *J. Catal.* **193**, 273 (2000).
8. Bernal, S., Calvino, J. J., Cifredo, G. A., and Rodriguez-Izquierdo, J. M., *J. Phys. Chem.* **99**, 11794 (1995).
9. Trovarelli, A., Dolcetti, G., de Leitenburg, C., Kaspar, J., Finetti, P., and Santoni, A., *J. Chem. Soc., Faraday Trans.* **88**, 1311 (1992).
10. Bernal, S., Calvino, J. J., Cifredo, G. A., Laachir, A., Perrichon, V., and Herrmann, J. M., *Langmuir* **10**, 717 (1994).
11. de Leitenburg, C., Trovarelli, A., and Kaspar, J., *J. Catal.* **166**, 98 (1997).
12. Sohlberg, K., Pantelides, S. T., and Pennycook, S. J., *J. Am. Chem. Soc.* **123**, 6609 (2001).
13. Badri, A., Binet, C., and Lavalley, J.-C., *J. Chem. Soc., Faraday Trans.* **96**, 4669 (1996).
14. Lamonier, C., Wrobel, G., and Bonnelle, J. P., *J. Mater. Chem.* **4**, 1927 (1994).
15. Perrichon, V., Laachir, A., Bergeret, G., Fréty, R., and Tournayan, L., *J. Chem. Soc., Faraday Trans.* **90**(5), 773 (1994).
16. Fierro, J. L. G., Soria, J., Sanz, J., and Rojo, J. M., *J. Solid State Chem.* **66**, 154 (1987).
17. Munuera, G., Fernandez, A., and Gonzalez-Elipe, A. R., *Stud. Surf. Sci. Catal.* **71**, 207 (1991).
18. Kondarides, D. I., and Verykios, X. E., *J. Catal.* **174**, 52 (1998).
19. Force, C., Belzengui, J. P., Sanz, J., Martinez-Arias, A., and Soria, J., *J. Catal.* **197**, 192 (2001).
20. Bernal, S., Blanco, G., Botana, F. J., Gatica, J. M., Pérez Omil, J. A., Pintado, J. M., Rodríguez-Izquierdo, J. M., Maestro, P., and Braconnier, J. J., *J. Alloys Compd.* **207**, 196 (1994).
21. Logan, A. D., and Shelef, M., *J. Mater. Res.* **9**, 468 (1994).
22. Balducci, G., Fornasiero, P., Di Monte, R., Kaspar, J., Meriani, S., and Graziani, M., *Catal. Lett.* **33**, 125 (1995).
23. Pijolat, M., Prin, M., Soustelle, M., Touret, O., and Nortier, P., *J. Chem. Soc., Faraday Trans.* **91**, 3941 (1995).
24. Fornasiero, P., Di Monte, R., Ranga Rao, G., Kaspar, J., Meriani, S., Trovarelli, A., and Graziani, M., *J. Catal.* **151**, 168 (1995).
25. Trovarelli, A., de Leitenburg, C., and Dolcetti, G., *CHEMTECH* **27**, 32 (1997).
26. Trovarelli, A., Zamar, F., Llorca, J., de Leitenburg, C., Dolcetti, G., and Kiss, J., *J. Catal.* **169**, 490 (1997).
27. Boaro, M., de Leitenburg, C., Dolcetti, G., and Trovarelli, A., *J. Catal.* **193**, 338 (2000).
28. Madier, Y., Descorme, C., Le Govic, A. M., and Duprez, D., *J. Phys. Chem. B* **103**, 10999 (1999).
29. Rocchini, E., Trovarelli, A., Llorca, J., Graham, G. W., Weber, W. H., Maciejewski, M., and Baiker, A., *J. Catal.* **194**, 461 (2000).
30. Vidal, H., Kaspar, J., Pijolat, M., Colon, G., Bernal, S., Cordon, A., Perrichon, V., and Fally, F., *Appl. Catal., B: Environ.* **27**, 49 (2000).
31. Sauvion, G.-N., Caillod, J., and Gourlaouen, C., U.S. Patent 4,940,685 (1990).
32. Bonneau, L., Chopin, T., and Touret, O., U.S. Patent 5,529,969 (1996).
33. Zotin, F. M. Z., Tournayan, L., Varlaud, J., Perrichon, V., and Frety, R., *Appl. Catal., A: General* **98**, 99 (1993).
34. Fornasiero, P., Hickey, N., Kaspar, J., Montini, T., and Graziani, M., *J. Catal.* **189**, 339 (2000).
35. Bernal, S., Botana, F. J., Calvino, J. J., Cauqui, M. A., Cifredo, G. A., Jobacho, A., Pintado, J. M., and Rodríguez-Izquierdo, J. M., *J. Phys. Chem.* **97**, 4118 (1993).
36. Fornasiero, P., Kaspar, J., Sergo, V., and Graziani, M., *J. Catal.* **182**, 56 (1999).
37. Graham, G. W., Jen, H.-W., Chun, W., and McCabe, R. W., *J. Catal.* **182**, 228 (1999).
38. Bernal, S., Calvino, J. J., Cauqui, M. A., Gatica, J. M., Larese, C., Pérez Omil, J. A., and Pintado, J. M., *Catal. Today* **50**, 175 (1999).
39. Lieske, H., Lietz, G., Spindler, H., and Völter, J., *J. Catal.* **81**, 8 (1983).
40. Bernal, S., Blanco, G., Calvino, J. J., Cifredo, G. A., Pérez Omil, J. A., Pintado, J. M., and Varo, A., *Stud. Surf. Sci. Catal.* **82**, 507 (1994).
41. Hickey, N., Fornasiero, P., Di Monte, R., Kaspar, J., Graziani, M., and Dolcetti, G., *Catal. Lett.* **72**, 45 (2001).
42. Bunluesin, T., Cordatos, H., and Gorte, R. J., *J. Catal.* **157**, 222 (1995).
43. Hwang, J. H., and Mason, T. O., *Z. Phys. Chem.* **207**, 21 (1998).
44. Bernal, S., Blanco, G., Calvino, J. J., Lopez-Cartez, C., Perez-Omil, J. A., Gatica, J. M., Stephan, O., and Colliex, C., *Catal. Lett.* **76**, 131 (2001).